NANO · MICRO small
www.small-journal.com

An Ultra-Simple Charge Supplementary Strategy for High Performance Rotary Triboelectric Nanogenerators

*Hongqing Feng, Yuan Bai, Lei Qiao, Zhe Li, Engui Wang, Shengyu Chao, Xuecheng Qu, Yu Cao, Zhuo Liu, Xi Han, Ruizeng Luo, Yizhu Shan, and Zhou Li**

Free-standing rotary triboelectric nanogenerators (rTENG) can accomplish special tasks which require both high voltage and high frequency. However, the reported high performance rTENG all have complex structures for output enhancement. In this work, an ultra-simple strategy to build high performance rTENG is developed. With only one small paper strip added to the conventional structure, the output of the TENG is promoted hugely. The voltage is triplicated to 2.3 kV, and the current and charge are quintupled to 133 μA and 197 nC, respectively. The small paper strip, with the merits of ultra-simplicity, wide availability, easy accessibility and low cost, functions as a super-effective charge supplement. This simple and delicate structure enables ultra-high durability with the 2.3 kV voltage output 100% maintained after 1 000 000 cycles. This charge supplementary strategy is universally effective for many other materials, and decouples the output enhancement from any friction or contact on the metal electrodes, emphasizing a critical working principle for the rTENG. Atmospheric cold plasma is generated using the paper strip rTENG (ps-rTENG), which demonstrates strong ability to do bacteria sterilization. This simple and persistent charge supplementary strategy can be easily adopted by other designs to promote the output even further.

1. Introduction

High voltage power supply is specially demanded in certain biological and environmental applications, including cell membrane electroporation,[1,2] mass spectrometry measurement,[3–5] plasma generation,[6–10] and dielectrophoresis in oil.[11,12] However, conventional high voltage power devices require large energy consumptions and raise critical safety concerns. Recently, Triboelectric nanogenerators (TENG) have been demonstrated to be effective energy harvesters in converting mechanical energy to electricity.[13–19] More importantly, they can generate high voltages of hundreds and even thousands of volts while the currents are at milliamp level, alleviating the energy cost and safety concerns in applications.[20–26]

Among the four typical modes of TENG,[13,22,27–33] the free-standing rotary TENG (rTENG) is unique, because they can achieve both high voltage and high

Prof. H. Q. Feng, Y. Bai, E. Wang, S. Y. Chao, X. C. Qu, Y. Z. Shan, Prof. Zhou Li
CAS Center for Excellence in Nanoscience
Beijing Key Laboratory of Micro–Nano Energy and Sensor
Beijing Institute of Nanoenergy and Nanosystems
Chinese Academy of Sciences
Beijing 100083, China
E-mail: zli@binn.cas.cn

Prof. H. Q. Feng, S. Y. Chao, X. C. Qu, Y. Z. Shan, Prof. Zhou Li
School of Nanoscience and Technology
University of Chinese Academy of Sciences
Beijing 100049, China

Y. Bai, E. Wang, Y. Cao, X. Han, R. Z. Luo, Prof. Zhou Li
Center of Nanoenergy Research
School of Physical Science and Technology
Guangxi University
Nanning 530004, China

Y. Bai, X. Han, R. Z. Luo
College of Chemistry and Chemical Engineering
Guangxi University
Nanning 530004, China

Dr. L. Qiao
Xuanwu Hospital Capital Medical University
Beijing 100053, China

Dr. Zhe Li
Institute of Engineering Medicine
School of Life Science
Beijing Institute of Technology
Beijing 100081, China

E. Wang
School of Resources
Environment and Materials
Guangxi University
Nanning 530004, China

Dr. Z. Liu
Beijing Advanced Innovation Centre for Biomedical Engineering
Key Laboratory for Biomechanics and Mechanobiology
of Ministry of Education
School of Biological Science and Medical Engineering
Beihang University
Beijing 100191, China

The ORCID identification number(s) for the author(s) of this article can be found under https://doi.org/10.1002/smll.202101430.

DOI: 10.1002/smll.202101430

frequency at the same time.[34,35] rTENG can be classified into two types, contact and non-contact ones.[36,37] The abrasions of contact rTENG are very severe, because the two friction layers keep on sliding against each other at high frequency. The abrasions of non-contact TENG can be avoided, but the output are less than the contact ones. To build high performance rTENG without abrasion drawbacks, charge pumping strategies are developed by several groups.[38–44] Bai et al. develop a coaxial and synchronous rotation structure that enables bound charges injection from the pumping rTENG to the main TENG via a rectifier.[39] Lei et al. design a different charge pumping rTENG consisting of three main components, a pair of rotatory disks, a polarizer, and a pair of accumulators.[42] Zhou et al. propose interfacial lubrication strategies between the frictional layer and electrode layer to reduce frictional loss of sliding rTENG.[45] These designs are capable to promote the voltage output of rotatory rTENG, but they all require very complicated structures as the charge sources.

In this work, an ultra-simple charge supplementary strategy to build high performance rTENG is developed. By simply adding one small paper strip to the classic non-contact rTENG structure, paper strip rTENG (ps-rTENG) is constructed, and the output is greatly enhanced. The voltage is promoted to over 2.3 kV, more than triplicated as before. In addition, the current and charge are more than quintupled. Although the output enhancement is huge, the friction between the paper strip and the dielectric layer is slight, which enables a 100% maintained output enhancement after 1 000 000 cycles. This charge supplementary strategy works uniquely for the dielectric layer. If the paper strip is reversed to make friction with the metallic layer, the output enhancement won't take place. This supplementary strategy is universally effective, as the output enhancement can be achieved using many other materials, not only paper. Employing this ultra-simple charge supplementary strategy, atmospheric cold plasma is generated using the ps-rTENG, and very effective bacteria sterilization is demonstrated.

2. Results

2.1. Structure Design and Working Principle

The structural scheme of the ps-rTENG is illustrated in **Figure 1**a, and the photos of the fabricated device are shown in Figure 1b and Figure S1 (Supporting Information). The device is mainly a classic non-contact rTENG, the only difference is that a small towel paper strip is folded and taped at the gap between two Al foil electrodes. By adjusting the distance between the stator and rotor, the ridge of the folded paper will get contact with the Polytetra fluoroethylene (PTFE) layers. Once started rotation, the paper ridge will make friction with the PTFE layer, but there are no friction between the PTFE and Al layers. Because the paper strip is soft and conformable, the friction between the paper strip and the PTFE film is very slight. The working mechanism of the ps-rTENG is illustrated in Figure 1c. Before the PTFE film and the paper strip contact each other, there are only electrostatic induction between PTFE

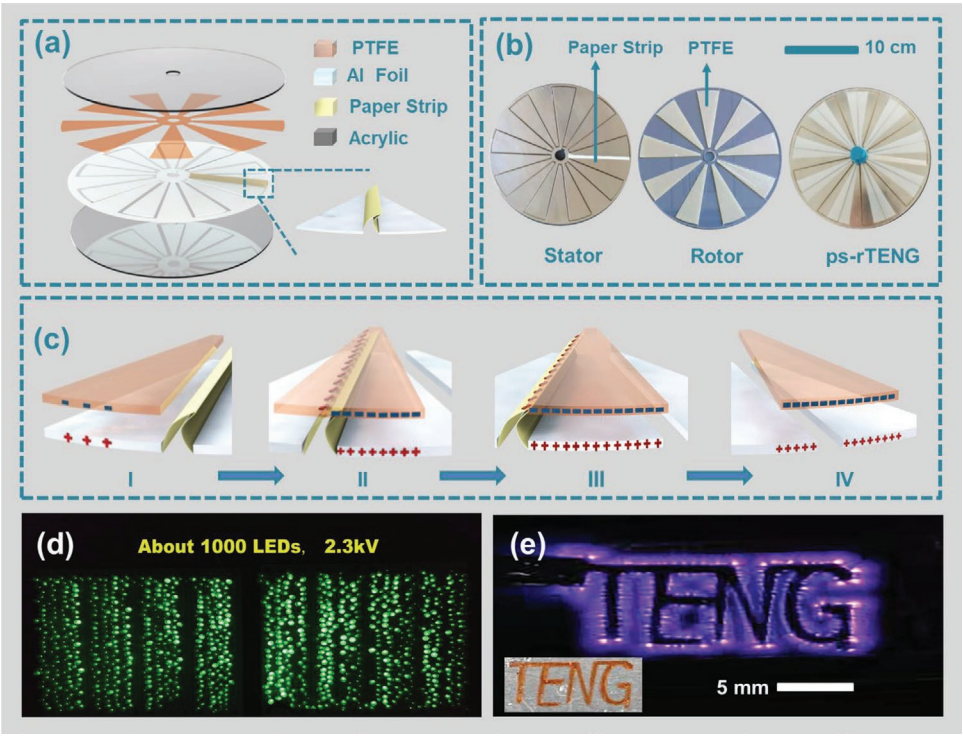

Figure 1. Structural design and operating mechanism of the ps-rTENG: a) schematic diagram of the ps-rTENG; b) photos of the stator and rotor, and the integrated device of the ps-rTENG; c) working principle of the ps-rTENG: the paper strip makes gentle friction with the PTFE film while rotating, and supplements huge amount of charges to the system, enabling great output enhancement; d) about 1000 LEDs (rated voltage: 3 V) are lighted up by the ps-rTENG; e) plasma generation using a patterned TENG electrode driven by ps-rTENG; inset: photo of the patterned electrode.

and Al electrodes, and only a few surface charges are induced at the Al electrodes (Figure 1c-I). After the PTFE and paper strip get touched and make friction against each other, many more negative charges are generated on the PTFE layer (Figure 1c-II). Consequently, more positive charges are induced on the Al electrodes (Figure 1c-III). As the PTFE keeps on rotating, much larger amount of charges are exchanged between pairs of the Al electrodes via external circuit, and the output of the rTENG are hugely promoted (Figure 1c-IV). Due to the promoted high voltage, about 1000 LEDs (rated voltage: 3 V) are lighted up using the ps-rTENG (Figure 1d), and atmospheric cold plasma is generated (Figure 1e).

2.2. Performance Characterization

Before the addition of the paper strip, the PTFE and Al layers produce a peak voltage of 702 V, peak current of 25 μA, and charge of 36 nC, at a rotation speed of 600 rpm and a distance of 2 mm (**Figure 2**a). After introducing the paper strip, the outputs are largely promoted to peak voltage of 2352 V, peak current of 133 μA, and charge of 197 nC. The rotation and the outputs are steady (Video S1, Supporting Information). The voltage is more than three folds over the previous one, and the current and charge are more than five folds (Figure 2b). These results demonstrate that the slight friction between the paper strip and

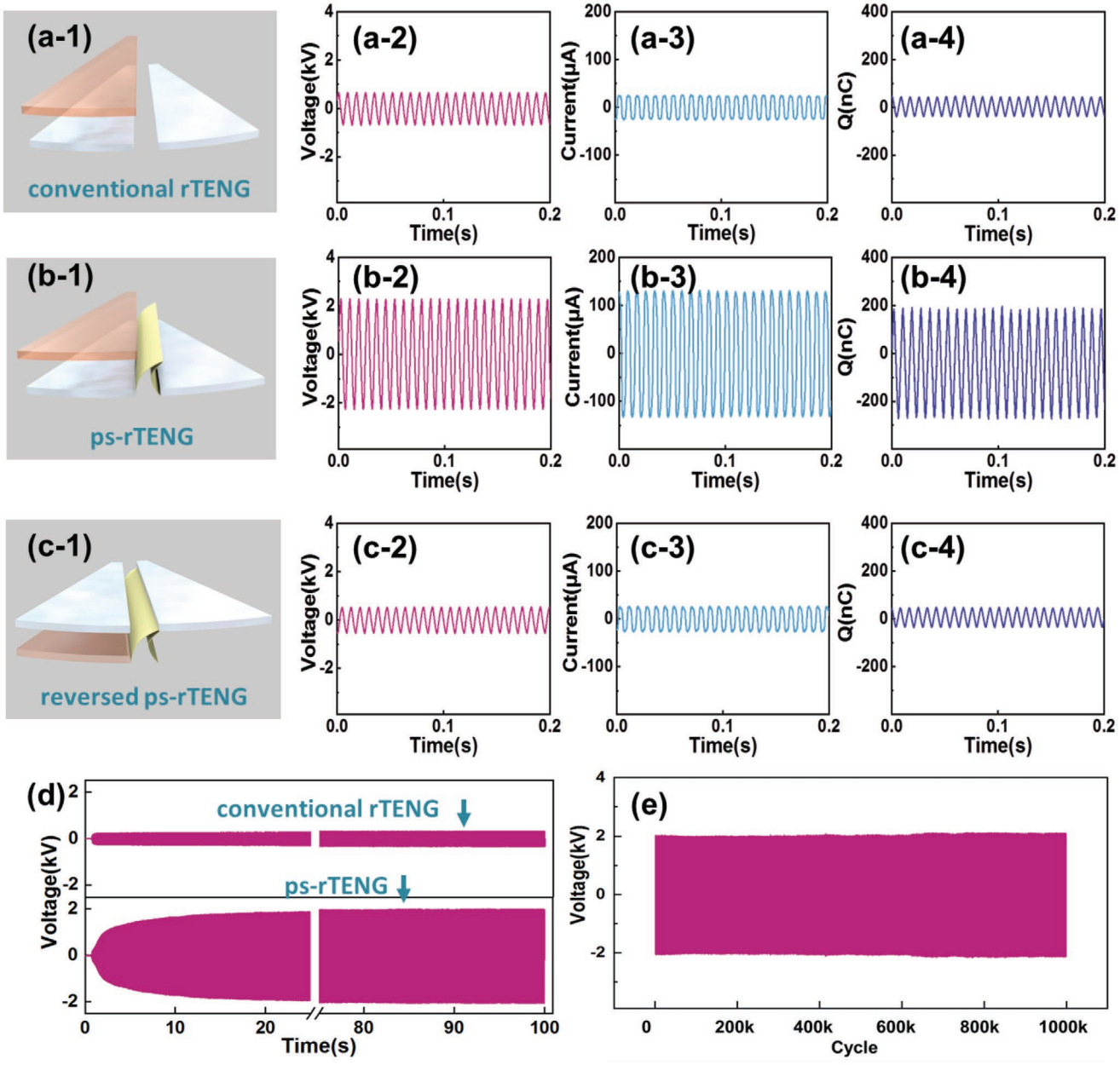

Figure 2. Electrical characteristics of the ps-rTENG. The schematic diagram (1), voltage (2), current (3), and charge (4) of the conventional a) rTENG, b) the ps-rTENG, and the c) reversed ps-rTENG; d) voltage evolution of the conventional rTENG, and ps-rTENG from 0 to 100 s; e) stability test of the ps-rTENG under continuous operation for 1000k cycles.

PTFE film accomplish great charge supplement to the device and successfully enhance the output to a great amount. The paper strip enables such effective charge supplementary to the rTENG device because PTFE and paper have distinct tendency to become charged. PTFE tends to be negatively charged, and paper tends to be positively charged.[46] The friction between the two produce much more negative charges on the PTFE film, and in consequence more positive charges are induced on the Al electrodes. Meanwhile, charge generation also takes place in the paper strip. When copper film is taped on the back of the paper strip, and connected to the ground, the peak voltage, peak current, and charge transfer between the two are measured to be 814 V, 12 μA, and 9 nC, respectively (Figure S2, Supporting Information). If the position of the paper strip is reversed to make friction with the Al layer, however, no output enhancement can be achieved. The voltage, current and charge are just the same as before (Figure 2c). These results verify the critical mechanisms and sequences of the output enhancement: paper strip making friction with the dielectric layer; additional charges generated and accumulated in the dielectric layer; more charges induced in the metal electrodes; and finally the output enhancement. The V_{oc} when only the paper strip is used to make friction with the Al electrodes is 20 V, much smaller than the electrostatic induction effect caused by the PTFE; increasing the number of paper strips doesn't increase the V_{oc} (Figure S3, Supporting Information).

Figure 2d demonstrates the charge accumulation process of the ps-rTENG. For conventional rTENG, the max peak voltage is reached within 1 s. For the ps-rTENG, the peak voltage in each rotation cycle increases gradually. At 25 s, the peak voltage reaches 1870 V, 90% of the max value. After 75 s, the peak voltage exceeds 2 kV. Meanwhile, because the PTFE and paper strip only make slight friction, the charge supplement and output enhancement are very persistent. After having PTEF and paper strip continuously sliding against each other for 1 000 000 cycles, the voltage output is still 100% as before (Figure 2e). The abrasions of the PTFE and Al electrodes are very slight, as compared with the contact rTENG (Figure S4, Supporting Information).

Next, we investigate strips made from other materials, kapton, nylon, and PTFE itself. **Figure 3**a show that they all can realize output enhancement to above 2 kV. Kapton and nylon are also materials that tend to be positively charged, and they confirm the working principle of this charge supplementary strategy. Notably, a PTFE strip can also realize a peak voltage of over 2 kV after making friction with the PTFE film. This is because friction between the same materials can also cause charge separation after they contact each other.[47,48] Nevertheless, among them, paper strip produces the highest voltage, and paper is the most easily available and economic material. Therefore paper is selected for further investigation. Only 1 strip is enough to triplicate the voltage output. When increasing the paper strips to 3, 6, 9, and even 18, only very slight further increase are obtained (Figure 3b). This suggests that the friction between one strip and the PTFE film have supplemented enough charges to promote the output. When the distance between the PTFE and Al film is enlarged from 2 to 6 mm, the peak voltage output decreases from 2352 to 1194 V gradually (Figure 3c). This in further confirms the importance of friction between PTFE and paper strip from another aspect. The voltage output also depends on the rotation speed. When the rotation speed increases from 120 to 240 rpm, the peak voltage increases obviously from 950 to 2110 V. In the range from 240 to 600 rpm, however, the voltage enhancement slows down (Figure 3d). The impact of different resistances to the peak voltage, current, and power output of the ps-rTENG are shown in Figure 3e,f. As load resistance increases to more than 1 MΩ, the peak current decreases obviously. As load resistance increases to hundreds of mega ohms, the peak voltage attains 1.8 KV (Figure 3e). A peak power of 120 mW is achieved with a resistance of about 30 MΩ (Figure 3f). Different capacitors are charged using this ps-rTENG in a rectified circuit (Figure 3g), and the voltage curves are shown in Figure 3h. A capacitor of 22 μF can be charged to 4 V within 2 s, which is quicker than the reported charge accumulation rTENG device with a much more complexed structure.[42]

2.3. Atmospheric Cold Plasma Generated by the ps-rTENG

The high output and frequency of the ps-rTENG are employed to generate atmospheric cold plasma. The plasma luminescence has been shown in Figure 1e. Also, a schematic diagram of needle-plate corona plasma generation is shown in **Figure 4**a. Argon has a relatively low breakdown voltage, therefore argon is employed to initiate the discharge. Meanwhile, considering our final purpose to do bacteria sterilization, 5% O_2 is introduced to the gas flow to increase the production of reactive oxygen species (ROS). The photo of the plasma excitation is shown in Figure 4b and Videos S2 and S3 (Supporting Information), obvious plasma plume is generated by the ps-rTENG. Figure 4c,d shows the relationship between the voltage and current when generating the plasma. The main peak current is about 30 μA, and the peak voltage at the two plasma electrodes is about 1.9 kV (Figure 4c). In one full electric cycle (Figure 4d), there are up to 8 obvious pulsed peaks in the current and voltage, which indicate that the argon-oxygen mixed gas has been discharged by the local high electric field. The discharges in the voltage waveform are less obvious, and there are only two big pulsed peaks at the main peaks each, which are in correspondence with the two largest discharges in the current. The other discharges in the voltage are almost invisible. However, after local enlargement, clear voltage discharges which are exactly consistent with the current discharges are presented (Figure 4d).

2.4. Bacterial Sterilization Using the ps-rTENG Generated Plasma

Atmospheric cold plasma has been well demonstrated to do pathogenic bacteria and fungi killing very effectively.[49–52] The sterilization mechanisms lie in the rich ROS generated during plasma stimulation using oxygen containing gases.[53,54] In this work, the sterilization efficiency of the plasma excited by the ps-rTENG is investigated. With mixed argon (95% argon and 5% oxygen) as the working gas, ROS such as ozone, superoxide anion, singlet oxygen, hydrogen peroxide, and hydroxyl radicals

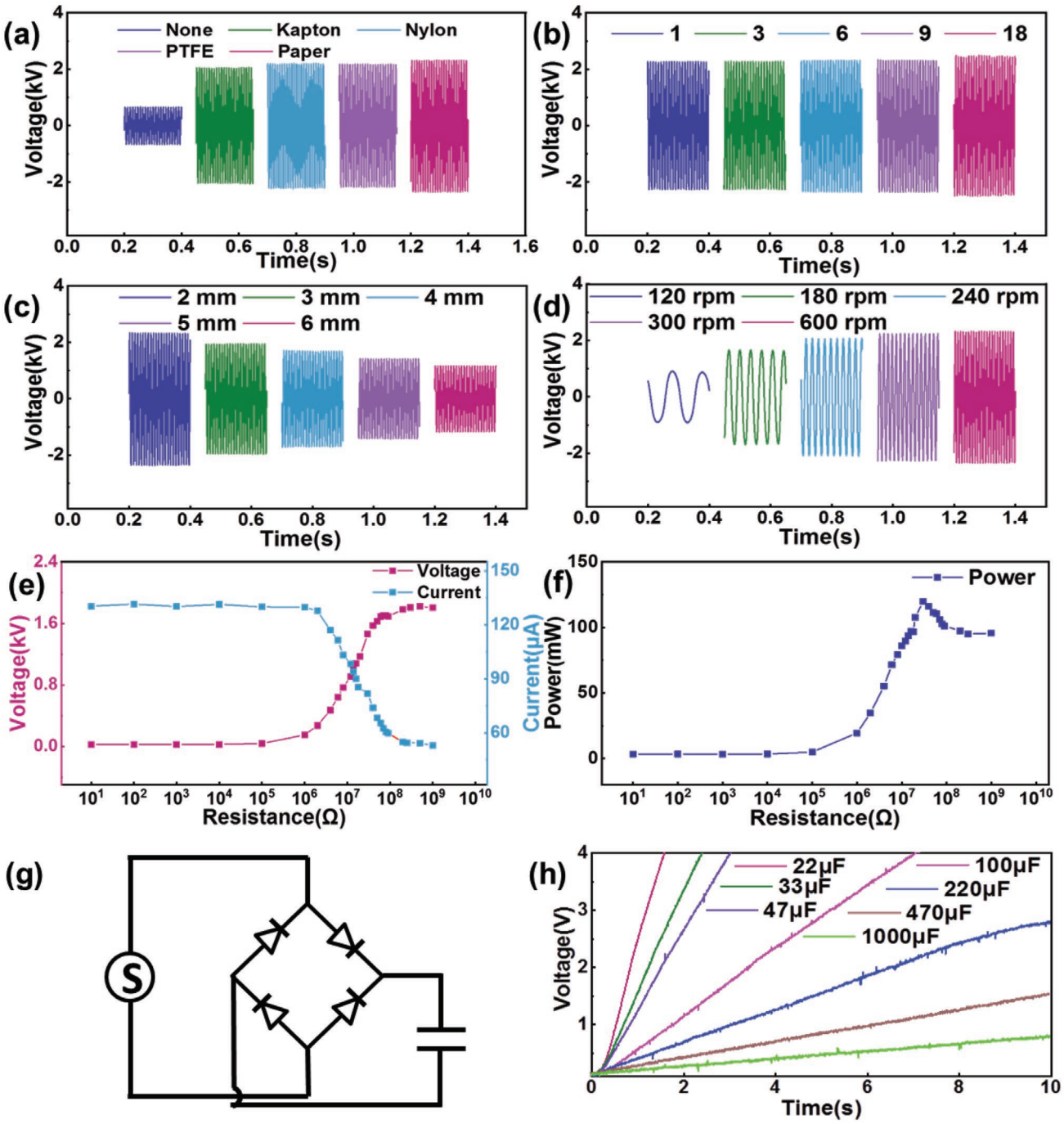

Figure 3. The influence of various factors on the voltage output of the ps-rTENG. a) Voltage of the ps-rTENG with different charge supplementary materials; b) voltage of the ps-rTENG versus the amount of paper strips; c) voltage of the ps-rTENG with different distance between PTFE and aluminum electrode; d) voltage of the ps-rTENG at different rotation speed; e) the variation of voltage and current and f) power of the ps-rTENG with different external load resistance; g) the circuit to do capacitor charging; h) voltage curves for different capacitors charged by the ps-rTENG.

are produced, as shown in the reaction Equations (1–7). These ROS endow plasma with strong ability to do bacteria killing.

$$Ar + e \rightarrow Ar^{*} + e \quad (1)$$

$$Ar + e \rightarrow Ar^{+} + 2e \quad (2)$$

$$O_2 + e \rightarrow 2O + e \quad (3)$$

$$2O_2 + O \rightarrow O_3 + O_2 \quad (4)$$

$$O_2 + e \rightarrow {}^{1}O_2 + e \quad (5)$$

$$2O_2^{-} + 2H_2O \rightarrow H_2O_2 + O_2 + 2OH^{-} \quad (6)$$

$$O_2^{-} + H_2O_2 \rightarrow \cdot OH + OH^{-} + O_2 \quad (7)$$

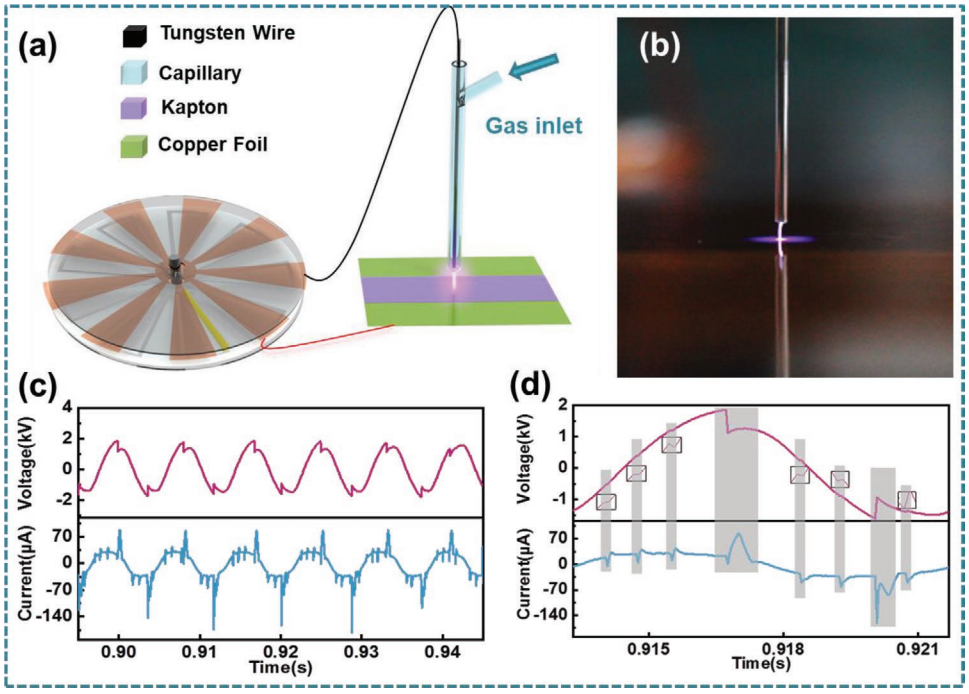

Figure 4. Needle-plate corona plasma generated by the ps-rTENG. a) Schematic diagram of the plasma excitation setup; b) photograph of the plasma; c) voltage and current during plasma generation in 0.05 s; d) voltage and current in one cycle.

The plasma excitation system is modified a little to adapt to the sterilization investigation, and the schematic diagram is shown in **Figure 5**a. Agar plate is used instead of kapton to help induce discharge, and it also serves as the growth support for the bacteria. As shown in Figure 5b and Video S4 (Supporting Information), plasma is successfully generated on the surface of the agar. 50 μL *Staphylococcus aureus (S. aureus)* with a concentration of 1×10^6 CFU mL^{-1} are added on the agar and a rectangle area of bacteria are formed using a cell spreader. To do plasma sterilization, the agar plate is moved under the plasma in a letter-writing route, as shown in Video S5 (Supporting Information). After 18 h culture, the bacteria on the untreated area grow into yellow colonies, and the colonies blend with each other forming a yellow rectangle on the agar. On the contrary, the bacteria in the plasma treated route have been completely killed, and no colonies grow. In this way the letters "TENG" and "NBL" are formed on the agar. These letters on the agar well demonstrate the bacterial sterilization ability of the ps-rTENG generated atmospheric plasma. If the letters are "written" with only gas flow without discharge, the bacteria in the writing route will not be influenced. They grow the same as those out of the writing route, and no letters can be formed (Figure S5, Supporting Information).

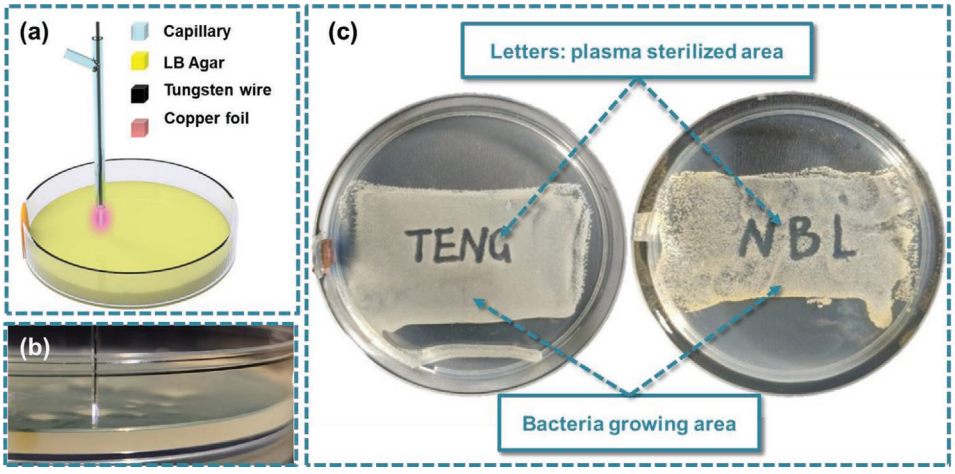

Figure 5. Bacterial sterilization using the ps-rTENG generated plasma. a) Schematic diagram of plasma excitation via ps-rTENG for bacterial sterilization; b) a photo of the plasma on the agar plate; c) photos of the "letters" on the agar plates after 18 h culture following bacterial sterilization.

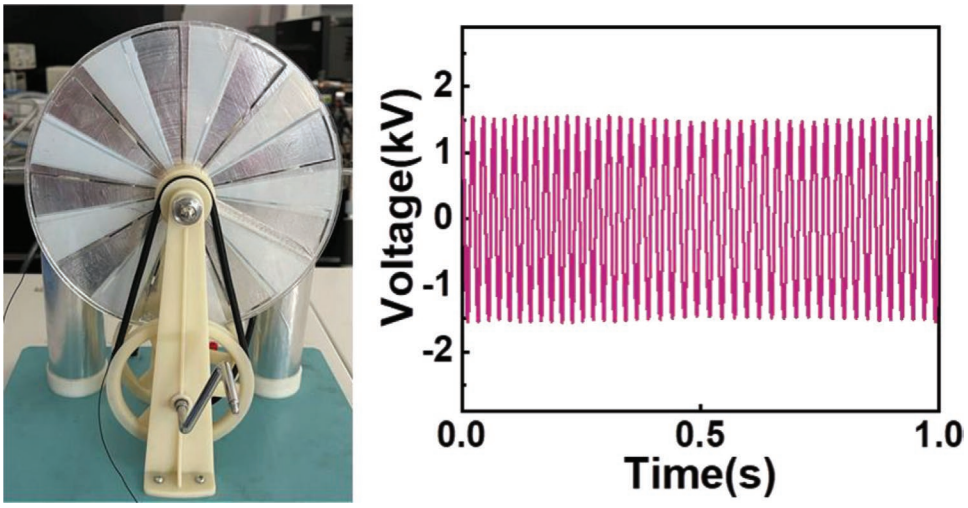

Figure 6. a) The ps-rTENG is installed in a manually driven device; and b) produces V_{oc} = 1.5 kV.

2.5. Manually Driven ps-rTENG for Plasma Generation

Apart from driven by a motor, the ps-rTENG can also be manually driven to do plasma generation. The ps-rTENG is installed in a device with a manual rocking bar, and V_{oc} of 1.5 kV is generated at a rotation speed of about 300 rpm (**Figure 6**). At this voltage, atmospheric plasma is successfully generated in air (Video S6, Supporting Information).

3. Discussion

In this paper, an ultra-simple strategy is developed for high performance rTENG by introducing one small paper strip to the conventional non-contact structure. The critical mechanism of this output enhancement strategy lies in the slight friction made on the dielectric layer (i.e., PTFE), which enables great amount of charge generation, accumulation and induction in the device. Owing to the small paper strip, the voltage is triplicated to 2.3 kV, and the current and charge are quintupled to 133 μA and 197 nC, respectively. On the contrary, additional friction made on the metal electrodes (i.e., Al) doesn't make any output enhancement. This work decouples output enhancement from friction or even contact on the metal electrodes, which provides important information for the rTENG structures and designs. Meanwhile, because the friction between the paper strip and the dielectric layer are very slight, the output enhancement is very persistent and 100% maintained after 1 000 000 cycles. With the help of this high output, atmospheric cold plasma is generated using the ps-rTENG, which is very effective in bacteria sterilization. We have also demonstrated plasma generation in air by manually driving the ps-rTENG. In future, with the help of some more dedicated rotation designs such as the pinwheel centrifuge,[55] it's very promising to realize more advanced manually driven ps-rTENG and replace the conventional high voltage power devices which have huge volume and safety concerns to do plasma excitation, making good use of both the high-voltage and self-powering merits of TENG. Last but not least, our charge supplementary strategy is extremely simple, which can be easily adopted by other systems such as the charge pumps[39] and charge accumulators[42] to promote the output of rTENG even further.

4. Experimental Section

Fabrication of the ps-rTENG and Electric Characteristics: The ps-rTENG has the same structure of a conventional rTENG: a stator, a rotor, and two layers on them each. Two acrylic disks (3 mm thick) with a diameter of 205 mm are fabricated using a laser cutting machine. Al foil (0.04 mm thick) with a diameter of 200 mm is divided into 18 sectors evenly and fixed as inner and outer ring electrodes on the stator acrylic disk. The gap between each sector is 2 mm. PTFE film (0.18 mm thick) is cut into 9 sectors with the same size as the stator sector and fixed on the rotor acrylic disk. A small rectangular paper strip (70 mm long, 10 mm wide) is cut from a paper towel and folded at the long centerline. The two long edges are taped at the gap between a pair of the Al sector electrodes. By doing this, a small piece of paper ridge is formed between the two Al electrodes. This paper strip serves as a charge supplement. By adjusting the distance between the stator and rotor, the paper ridge can get contact with the PTFE film, while the PTFE and Al electrodes are still separated from each other. A rotary motor with adjustable speed is used to drive the ps-rTENG. The open circuit voltage is measured using an oscilloscope (Teledyne LeCroy HD 4096). The short circuit current and charge are measured using an electrometer (Keithley 6517).

Atmospheric Cold Plasma Generation Using the ps-rTENG: To generate atmospheric cold plasma for luminescence, a "TENG" patterned electrode is fabricated by cutting Cu film. The patterned Cu electrode and the Al film electrode are separated by a piece of thin cover glass, and connected to the ps-rTENG each. To generate atmospheric cold plasma to do sterilization, a tungsten wire (Ø = 0.3 mm) is placed inside a capillary (Ø outer = 0.6 mm, Ø inner = 0.5 mm) as an electrode, and copper foil is taped on an acrylic plate as the other. The two electrodes are connected to the ps-rTENG. A kapton film is taped on the Cu foil as the dielectric layer for more steady plasma generation. The capillary with tungsten wire electrode is placed 2 mm above the kapton film. Argon mixture (95% argon + 5% oxygen) at a flow speed of 800 sccm is used as working gas.

Bacterial Sterilization Using the ps-rTENG Generated Plasma: *S. aureus* is cultured in Luria-Bertani (LB) medium (yeast extract 5 g L^{-1}, tryptone 10 g L^{-1}, and NaCl 10 g L^{-1} in deionized water, autoclaved). The plasma stimulation system is modified a little to adapt to the sterilization investigation. The ps-rTENG is connected to the tungsten wire in the

capillary tube and a copper foil, respectively. The copper foil is taped to the side wall of a petri dish. Then warm LB agar liquid (10 g agar powder in 1 L medium, autoclaved) is poured into the dish and let consolidate to form agar plate. 50 µL of 1×10^6 CFU mL^{-1} *S. aureus* is added at the center of the agar plate and spread into a rectangular area with a cell spreader. The dish is moved under the plasma plume in a letter-writing route. Then the plates are incubated at 37 °C for 18 h after plasma treatment.

Supporting Information

Supporting Information is available from the Wiley Online Library or from the author.

Acknowledgements

H.Q.F., Y.B., and L.Q. contributed equally to this work. This work is supported by National Natural Science Foundation of China (81971770, 61875015), China Postdoctoral Science Foundation (2020M680302), and Beijing Natural Science Foundation (JQ20038).

Conflict of Interest

The authors declare no conflict of interest.

Data Availability Statement

Research data are not shared.

Keywords

bacteria sterilization, charge supplement, high output, plasma, triboelectric nanogenerators

Received: March 11, 2021
Revised: April 13, 2021
Published online:

[1] A. Muralidharan, L. Rems, M. T. Kreutzer, P. E. Boukany, *Biochim. Biophys. Acta, Biomembr.* **2021**, *1863*, 183468.
[2] T. Kotnik, L. Rems, M. Tarek, D. Miklavčič, *Annu. Rev. Biophys.* **2019**, *48*, 63.
[3] M.-M. Chen, H.-F. Su, Y. Xie, L.-F. He, S.-C. Lin, M.-L. Zhang, C. Wang, S.-Y. Xie, R.-B. Huang, L.-S. Zheng, *Sci. Bull.* **2018**, *63*, 1351.
[4] N. A. Huizen, J. N. M. Ijzermans, P. C. Burgers, T. M. Luider, *Mass Spectrom. Rev.* **2019**, *39*, 309.
[5] Y. Yang, Y. Huang, J. Wu, N. Liu, J. Deng, T. Luan, *TrAC, Trends Anal. Chem.* **2017**, *90*, 14.
[6] K. Zhang, C. A. Perussello, V. Milosavljević, P. J. Cullen, D.-W. Sun, B. K. Tiwari, *Crit. Rev. Food Sci. Nutr.* **2019**, *59*, 812.
[7] T. Bernhardt, M. L. Semmler, M. Schäfer, S. Bekeschus, S. Emmert, L. Boeckmann, *Oxid. Med. Cell. Longevity* **2019**, *2019*, 1.
[8] N. Y. Babaeva, G. V. Naidis, *Trends Biotechnol.* **2018**, *36*, 603.
[9] H. Xie, P. Svenmarker, J. Axelsson, S. Gräfe, M. Kyriazi, N. Bendsoe, S. Andersson-Engels, K. Svanberg, *J. Biophotonics* **2015**, *8*, 142.
[10] R.-C. Qian, Y. Cao, L.-J. Zhao, Z. Gu, Y.-T. Long, *Angew. Chem., Int. Ed.* **2017**, *56*, 4802.
[11] Y. Zhou, B. Li, M. Zhang, Z. Sun, Z. Wang, J. Wang, *Chem. Eng. Sci.* **2020**, *224*, 115739.
[12] M. T. Rabbani, C. F. Schmidt, A. Ros, *Anal. Chem.* **2017**, *89*, 13235.
[13] F.-R. Fan, Z.-Q. Tian, L. Wang, *Nano Energy* **2012**, *1*, 328.
[14] H. Ouyang, Z. Liu, N. Li, B. Shi, Y. Zou, F. Xie, Y. Ma, Z. Li, H. Li, Q. Zheng, X. Qu, Y. Fan, Z. L. Wang, H. Zhang, Z. Li, *Nat. Commun.* **2019**, *10*, 1821.
[15] B. Shi, Z. Liu, Q. Zheng, J. Meng, H. Ouyang, Y. Zou, D. Jiang, X. Qu, M. Yu, L. Zhao, Y. Fan, Z. L. Wang, Z. Li, *ACS Nano* **2019**, *13*, 6017.
[16] T. Jiang, H. Pang, J. An, P. Lu, Y. Feng, X. Liang, W. Zhong, Z. L. Wang, *Adv. Energy Mater.* **2020**, *10*, 2000064.
[17] W. Zhong, L. Xu, F. Zhan, H. Wang, F. Wang, Z. L. Wang, *ACS Nano* **2020**, *14*, 10510.
[18] B. Dong, Q. Shi, T. He, S. Zhu, Z. Zhang, Z. Sun, Y. Ma, D. L. Kwong, C. Lee, *Adv. Sci.* **2020**, *7*, 1903636.
[19] H. Wang, M. Han, Y. Song, H. Zhang, *Nano Energy* **2021**, *81*, 105627.
[20] Y. Feng, Y. Zheng, G. Zhang, D. Wang, F. Zhou, W. Liu, *Nano Energy* **2017**, *38*, 467.
[21] C. Wu, H. Tetik, J. Cheng, W. Ding, H. Guo, X. Tao, N. Zhou, Y. Zi, Z. Wu, H. J. A. F. M. Wu, *Adv. Funct. Mater.* **2019**, *29*, 1901102.
[22] M. Bi, S. Wang, X. Wang, X. Ye, *Nano Energy* **2017**, *41*, 434.
[23] Y. Han, J. Zou, Z. Li, W. Wang, Y. Jie, J. Ma, B. Tang, Q. Zhang, X. Cao, S. Xu, Z. L. Wang, *ACS Nano* **2018**, *12*, 4835.
[24] G. Zhu, J. Chen, T. Zhang, Q. Jing, Z. L. Wang, *Nat. Commun.* **2014**, *5*, 3426.
[25] H. J. Yoon, M. Kang, W. Seung, S. S. Kwak, J. Kim, H. T. Kim, S. W. Kim, *Adv. Energy Mater.* **2020**, *10*, 2000730.
[26] J. Kim, H. Cho, M. Han, Y. Jung, S. S. Kwak, H. J. Yoon, B. Park, H. Kim, H. Kim, J. Park, S. W. Kim, *Adv. Energy Mater.* **2020**, *10*, 2002312.
[27] J. Chen, G. Zhu, W. Yang, Q. Jing, P. Bai, Y. Yang, T. C. Hou, Z. L. Wang, *Adv. Mater.* **2013**, *25*, 6094.
[28] S. Wang, L. Lin, Y. Xie, Q. Jing, S. Niu, Z. L. Wang, *Nano Lett.* **2013**, *13*, 2226.
[29] Y. Yang, H. Zhang, J. Chen, Q. Jing, Y. S. Zhou, X. Wen, Z. L. J. A. N. Wang, *ACS Nano* **2013**, *7*, 7342.
[30] S. Wang, Y. Xie, S. Niu, L. Lin, Z. L. Wang, *Adv. Mater.* **2014**, *26*, 2818.
[31] H. S. Wang, C. K. Jeong, M.-H. Seo, D. J. Joe, J. H. Han, J.-B. Yoon, K. J. Lee, *Nano Energy* **2017**, *35*, 415.
[32] W. Song, B. Gan, T. Jiang, Y. Zhang, A. Yu, H. Yuan, N. Chen, C. Sun, Z. L. Wang, *ACS Nano* **2016**, *10*, 8097.
[33] Y. Mao, D. Geng, E. Liang, X. Wang, *Nano Energy* **2015**, *15*, 227.
[34] L. Lin, S. Wang, Y. Xie, Q. Jing, S. Niu, Y. Hu, Z. L. Wang, *Nano Lett.* **2013**, *13*, 2916.
[35] T. Jiang, X. Chen, C. B. Han, W. Tang, Z. L. Wang, *Adv. Funct. Mater.* **2015**, *25*, 2928.
[36] L. Lin, S. Wang, S. Niu, C. Liu, Y. Xie, Z. L. Wang, *ACS Appl. Mater. Interfaces* **2014**, *6*, 3031.
[37] D. Jiang, H. Ouyang, B. Shi, Y. Zou, P. Tan, X. Qu, S. Chao, Y. Xi, C. Zhao, Y. Fan, Z. Li, *InfoMat* **2020**, *2*, 1191.
[38] W. Liu, Z. Wang, G. Wang, G. Liu, J. Chen, X. Pu, Y. Xi, X. Wang, H. Guo, C. Hu, Z. L. Wang, *Nat. Commun.* **2019**, *10*, 1426.
[39] Y. Bai, L. Xu, S. Lin, J. Luo, H. Qin, K. Han, Z. L. Wang, *Adv. Energy Mater.* **2020**, *10*, 2000605.
[40] H. Wang, L. Xu, Y. Bai, Z. L. Wang, *Nat. Commun.* **2020**, *11*, 11.
[41] X. Liang, T. Jiang, Y. Feng, P. Lu, J. An, Z. L. Wang, *Adv. Energy Mater.* **2020**, *10*, 2002123.
[42] R. Lei, Y. Shi, Y. Ding, J. Nie, S. Li, F. Wang, H. Zhai, X. Chen, Z. L. Wang, *Energy Environ. Sci.* **2020**, *13*, 2178.
[43] L. Xu, T. Z. Bu, X. D. Yang, C. Zhang, Z. L. Wang, *Nano Energy* **2018**, *49*, 625.
[44] L. Xu, H. Wu, G. Yao, L. Chen, X. Yang, B. Chen, X. Huang, W. Zhong, X. Chen, Z. Yin, Z. L. Wang, *ACS Nano* **2018**, *12*, 10262.

[45] L. Zhou, D. Liu, Z. Zhao, S. Li, Y. Liu, L. Liu, Y. Gao, Z. L. Wang, J. Wang, *Adv. Energy Mater.* **2020**, *10*, 2002920.
[46] H. Zou, Y. Zhang, L. Guo, P. Wang, X. He, G. Dai, H. Zheng, C. Chen, A. C. Wang, C. Xu, Z. L. Wang, *Nat. Commun.* **2019**, *10*, 1427.
[47] H. Y. Li, L. Su, S. Y. Kuang, C. F. Pan, G. Zhu, Z. L. Wang, *Adv. Funct. Mater.* **2015**, *25*, 5691.
[48] L. Lapčinskis, K. Mālnieks, A. Linarts, J. Blūms, K. n. Šmits, M. Järvekülg, M. r. Knite, A. Šutka, *ACS Appl. Energy Mater.* **2019**, *2*, 4027.
[49] Q. Zhang, P. Sun, H. Feng, R. Wang, Y. Liang, W. Zhu, K. H. Becker, J. Zhang, J. Fang, *J. Appl. Phys.* **2012**, *111*, 123305.
[50] H. Feng, P. Sun, Y. Chai, G. Tong, J. Zhang, W. Zhu, J. Fang, *IEEE Trans. Plasma Sci.* **2009**, *37*, 121.
[51] H. Liu, J.-j. Li, Z.-r. Li, K. Xu, Z.-j. Chen, G.-c. Chen, *Crystals* **2019**, *9*, 32.
[52] P. P. Sun, R. Zhang, W. Chen, P. V. Braun, J. Gary Eden, *Appl. Phys. Rev.* **2019**, *6*, 041406.
[53] H. Feng, R. Wang, P. Sun, H. Wu, Q. Liu, J. Fang, W. Zhu, F. Li, J. Zhang, *Appl. Phys. Lett.* **2010**, *97*, 131501.
[54] H. Wu, P. Sun, H. Feng, H. Zhou, R. Wang, Y. Liang, J. Lu, W. Zhu, J. Zhang, J. Fang, *Plasma Processes Polym.* **2012**, *9*, 417.
[55] M. S. Bhamla, B. Benson, C. Chai, G. Katsikis, A. Johri, M. Prakash, *Nat. Biomed. Eng.* **2017**, *1*, 1.